Aerospace Science and Technology 28 (2013) 9–20

Contents lists available at SciVerse ScienceDirect

Aerospace Science and Technology

www.elsevier.com/locate/aescte

A new bird model and the effect of bird geometry in impacts from various orientations

Reza Hedayati *, Saeed Ziaei-Rad

Mechanical Engineering Department, Isfahan University of Technology, Isfahan 84156-83111, Iran

ARTICLE INFO

Article history:
Received 14 July 2011
Received in revised form 1 August 2012
Accepted 18 September 2012
Available online 5 October 2012

Keywords:
Bird strike
SPH method
Bird orientation
Realistic bird model
Bufflehead duck
Ellipsoid shaped bird model

ABSTRACT

In this paper, a bird model with geometry similar to a real bird (Bufflehead Duck) is introduced and compared to traditional bird models and also to experimental data. A bird can impact a part of an airplane from its head, tail, bottom or wings. Any of these orientations can have a different effect on the response of an airplane part. Since all birds do not have the same body shapes and sizes, and, since, it is not always convenient to model a complex bird body, four substitute bird models are introduced. The models results are then compared in order to determine the best substitute bird which can properly model the pressure and force exerted by real birds when impacting from different orientations. It was concluded that the impact from bird bottom side is the most damaging scenario, while the tail side impact is the less dangerous one. It was also found that for the tail side impact scenario, a hemispherical-ended cylinder shows the best results, while for the bottom side impact scenario, an ellipsoid can be the best candidate for the bird substitute model.

1. Introduction

Bird strike is a common hazard for flight safety that causes remarkable losses every year. Statistics indicate that although all aircraft designs have to be certified for a level of bird impact resistance, the number of bird strikes has been increasing every year [5]. This can be attributed to globalization which has resulted in the steady increase in air traffic density levels as well as the dramatic expansion of wild bird populations [5]. Based on the Federal Aviation Administration National Wildlife Strike Database [25], during the years 1912 to 2004, there were 47 fatal bird strike accidents that have killed 242 people. The total number of aircraft destroyed due to the bird strike in that period was 90. Bird strike costs the U.S. civil aviation industry more than $495 million yearly [5].

An aircraft must show compliance with "continued safe flight and landing" requirements following specified types of high-energy bird impact. Experimental tests for bird strike certification are very expensive and time consuming. In order to decrease the number of costly sample tests, a trustworthy analysis tool is necessary to reliably predict the structural responses of bird and target. The use of Finite Element (FE) simulation provides the opportunity to effectively evaluate numerous structural design approaches that minimize structural weight and reduce the risk of not meeting civil or military bird strike design requirements. However, analysis techniques must be validated before they can be employed to accurately guide the design process.

In the absence of high-tech computers, Barber et al. [2] performed numerous bird impact tests on a rigid target plate. He used birds with different body shapes, weights, etc. He found out that the peak pressures generated on the center of the target plate due to bird impact is independent of the bird size and is proportional to the square of the impact velocity. Niering used Lagrangian method to model the bird impact phenomenon [21]. He used different finite element methods in his work, but finally stated that refinements in the models are necessary due to high distortion of bird elements during the impact. Stoll and Brockman tried to overcome the problem by eliminating highly distorted elements [24]. This, however, leads to the bird mass loss during the impact. Due to Lagrangian method disadvantages, some authors used other approaches like Arbitrary Lagrangian–Eulerian (ALE) for modeling bird behavior during the impact. Moffat and Cleghorn implemented the MSC/DYTRAN code to develop a bird model for an ALE description [19]. They reproduced the impacts of the bird in rigid and flexible targets. Hanssen et al. also used the ALE approach to study the bird impact against aluminum foam-based sandwich panels [8].

Another approach to study the bird strike simulation is a meshless method called Smoothed Particles Hydrodynamics (SPH). Hutt et al. introduced the SPH method, showed its utilization and provided comprehensive data of its computational parameters [9]. Martin studied a transient, material, and geometric nonlinear finite element based impact analysis using PW/WHAM [16]. He used

* Corresponding author. Tel.: +98 311 3915244; fax: +98 311 3912628.
E-mail addresses: rezahedayati@gmail.com (R. Hedayati), szrad@cc.iut.ac.ir (S. Ziaei-Rad).

1270-9638/$ – see front matter
http://dx.doi.org/10.1016/j.ast.2012.09.002

Fig. 1. A flock of birds striking an airplane wing (courtesy of Juergen Kienast/Bild).

a formulation very similar to the concept of SPH technique. Ubels et al. also used the SPH method to simulate the bird strike against airplane wing leading edge structure [26]. They employed the PAM-CRASH code to model the bird using SPH elements and the impacted structure using Lagrangian elements.

Researchers have used three simple configurations to model the bird in a bird strike event. By reviewing the literature, it was found out that the effect of implementing a realistic bird model has not been investigated so far. As a result in this paper, a bird model with geometry similar to a real bird (Bufflehead Duck) is introduced and compared to traditional bird models and also to the experimental data. There are different bird types with different body shapes; but most have an ellipsoid shaped torso with a round head much smaller than their torso. Although there are many different types of birds, the obtained results can be extended to other bird species in a qualitative way. Modeling a bird with a realistic body shape also makes possible to investigate the effect of bird orientations in the bird strike on structures. When not many investigations have been carried out on the effect of orientation a bird impacts a surface, it can be an important factor. It is because in the real bird strike events the birds do not always impact a surface from the same orientation. Fig. 1 shows a real situation in which a flock of birds with different orientations are going to strike an airplane. A bird can impact a part of an airplane from its head, tail, bottom or wings. Any of these orientations can have a different effect on the integrity of airplane parts. The results are then compared to the traditional bird strike simulations as well as experimental results published by Wilbeck [27]. Since all birds do not have the same body shapes and sizes, and since, it is not always convenient to model a complex bird body, four substitute bird models are introduced. The model results are then compared in order to determine the best substitute bird which can best model the pressure and force exerted by real birds when impacting from different orientations. In the present study, all the specifications for simulations are similar to traditional bird models used by other researchers, except for the geometry of the bird.

2. Numerical methods

Since the experimental verifications are time consuming, expensive and difficult to perform, numerical simulations can provide significant help in designing high-efficiency bird-proof structures. Explicit nonlinear finite element (FE) codes, which are available in several high-end commercial FE solvers, have been used to treat different problems of this class.

A bird strike is characterized by loads with high intensity and short duration. The materials undergo high strain rates, large deformations and inelastic strains. The constraint derived from the contacts and the elastic–plastic behavior considered for the material can be used to study the interaction between the bird and the target.

Since late eighties, FE codes adopted various finite element approaches to model the impact phenomena. These include the Lagrangian approach, Arbitrary Lagrangian–Eulerian (ALE) approach, and recent solvers based on Smoothed Particle Hydrodynamics (SPH).

Unlike the implicit technique, the explicit integration technique used in the bird strike analysis is conditionally stable, requiring the critical time step to meet the Courant criterion, which is ultimately determined by the smallest element size in the FE model. The advantage of Lagrangian method is its ease of use and also the ability to track history dependant materials. However, by using the Lagrangian approach for bird modeling, the element size tends to become very small and distorted. This ultimately results in prohibitive computational time and often produces an unstable numerical solution. In fact, in an explicit FE analysis, the time step Δt is determined by the characteristic length of the smallest element L:

$$\Delta t = \frac{L}{c} \tag{1}$$

where c is the wave propagation velocity in the material. Since severe mesh distortion decreases the smallest side size of element, it causes the time step to decrease to an excessively low value for the calculations to be continued.

The Arbitrary Lagrangian–Eulerian (ALE) formulation is a combination of the Lagrange and Eulerian formulations in which the reference is set arbitrarily by the user in order to capture the advantages of the methods while minimizing the disadvantages. The user must set the mesh motion that best suites the problem in order to minimize the mesh distortions and obtain the best results. The main disadvantage of this formulation is that the user must be experienced in order to select the best method, and interpret the results obtained. A very comprehensive description of the ALE method has been presented by Stoker [23].

SPH is a meshless method first introduced by Lucy [15]. It is a Lagrangian numerical technique used to solve the fluid equations of motion. Specifically, it uses an interpolation kernel of compact support to represent any field quantity in terms of its values as a set of disordered particles. The material is discretized, and properties of these nodes are associated with the center of the particles. A chosen interpolation kernel determines the amount of effect that a known point value contributes to the point of interest. The advantages of the SPH method is that first, it does not require element meshing and thus avoids mesh tangling; second, unlike the ALE method it does not require considering and setting many parameters and is less complex and; third, since in this paper the effect of orientation at which a bird impacts a surface is investigated, the different mesh size at different parts of a bird can affect the results. In the SPH method, the particles are described by:

$$\left(x_i(t), m_i(t)\right)_{i\in P} \tag{2}$$

where P is the set of moving particles and $x_i(t)$ and $m_i(t)$ are the location and the mass of each moving particle, respectively. The movement of each particle is related to the mass change by [10]:

$$\frac{dm_i}{dt} = \nabla.V(x_i, t)m_i \tag{3}$$

where V is the velocity of the particle i. Smoothing kernel is a valuable concept in SPH technique. Before presenting the smoothing kernel, auxiliary cubic B-spline function must be introduced:

$$\theta(y) = \alpha_1 \times \begin{cases} 1 - \frac{3}{2}y^2 + \frac{3}{4}y^3 & y \leqslant 1 \\ \frac{1}{4}(2-y)^3 & 1 \leqslant y \leqslant 2 \\ 0 & y \geqslant 2 \end{cases} \quad (4)$$

where α_1 is a constant depending on the dimension and the slope of kernel function. In two dimensions: $\alpha_1 = \frac{10}{7\pi}$.

Lacome suggested the smoothing kernel as [10]:

$$W(x_i - x_j, \bar{h}) = \frac{1}{\bar{h}}\theta\left(\frac{x_i - x_j}{\bar{h}}\right) \quad (5)$$

where $\bar{h}$ is the smoothing length. Initially, while using the SPH method, the smoothing length was considered constant during the entire simulation. However it has been shown that it is more appropriate for each particle to have its own smoothing particle depending on the number of neighbor particles. Therefore, in the above equations, $\bar{h}$ can be replaced by $h(x_i)$.

In 1989, Monaghan defined the mass density by [20]:

$$\rho(x_i) = \sum_{j=1}^{N} m_j W(x_i - x_j, \bar{h}) \quad (6)$$

The equation of conservation of mass in Lagrangian form is [20]:

$$\frac{d\rho}{dt}(x_i) = -\rho \nabla V \quad (7)$$

The SPH approximation for the conservation of mass can be written as [20]:

$$\frac{d\rho}{dt}(x_i) = \sum_{j=1}^{N} m_j \big(v(x_j) - v(x_i)\big)\nabla W_{ij} \quad (8)$$

The neighbor search is a very important step in the SPH computation. It is important to know at any time of the calculation which particle is going to interact with which other. The sphere of influence of each particle is a finite domain of a radius of 2 h. The goal of the neighbor search is to list the particle inside that domain at each time step. In a direct search for a set of N particles, the number of distance comparisons required is $N-1$. Since this comparison needs to be made for each particle, the total number of comparisons is $N(N-1)$ which can dominate the total CPU time for large models. The idea of the search for neighbors is to use the same algorithm than the one used for the contact search: the bucket sort. The domain covered by the particles is split in several boxes of a given size. Then for each particle, we search for neighbors inside the main box and also the neighbor boxes contained in the domain of influence of the given particle. Then, when the list of hypothetic neighbors is known, we compute the distance between each couple of particles and check if it is smaller than twice the smoothing length. The total cost of the grouping operations and comparisons, needed to form the buckets, can be nearly linear with the number of particles N [11].

Many researchers [6,12,17,1] have simplified the bird torso as a hemispherical-ended cylinder. The ellipsoid geometry is also a well-accepted choice, which has been suggested by the International Bird Strike Research Group [22], and has been used by Guan et al. [7]. Besides these two configurations, the straight-ended cylinder has also been adopted by Brockman and Held [3], but its application remains somewhat infrequent. Recently, Meguid et al. focused on the three most-frequently used configurations mentioned above: namely, hemispherical-ended cylinder, straight-ended cylinder, and ellipsoid, at various length-to-diameter aspect ratios [18]. The results of their study showed that the initial contact area between the bird and target in the early phase of the impact event would have a significant effect on the peak impact force. The aspect ratio of the bird striking both rigid panel and flexible fan blade was found to have little influence on the normalized impact force and impulse.

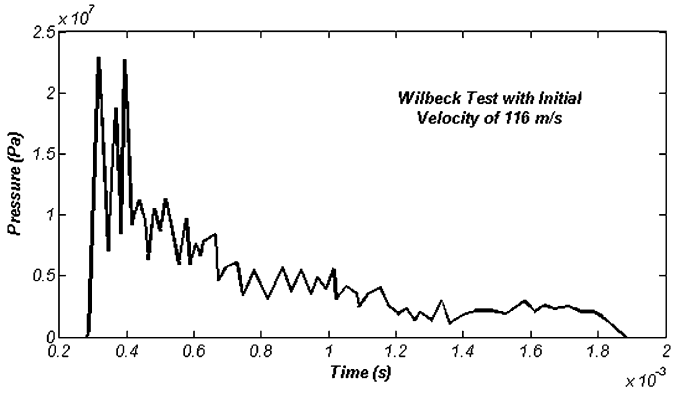

Fig. 2. Pressure profile at the center of impact from Wilbeck experimental test (1977).

3. Theoretical methods

Wilbeck was one of the first researchers who investigated the experimental behavior of a bird under impact [27]. His conclusions and results have kept their importance till now since most numerical case studies carried out by other researchers used the same shape and characteristics as used in Wilbeck's paper. Also, results from his experimental data were used as a reference for comparison with numerical results. Among Wilbeck's numerous tests, the impact of a real bird having an initial velocity of 116 $\mathrm{m\,s^{-1}}$ was selected for this study (see Fig. 2).

When a projectile of any material impacts a target plate, the particles on the front surface of the projectile are instantaneously brought to rest relative to the target face and a shock is formed. The purpose of this shock wave is to bring each succeeding layer of particles to rest. The pressure in the shock compressed region is very high initially and is constant throughout the region at early times. As the shock propagates up the projectile, the particles along the projectile's edge are subjected to a very high pressure gradient due to the shock loading on one side and the free surface on the other. This pressure gradient causes the particles to be accelerated radially outward and a release wave is formed.

If, at any time, the state of stress is such that the strength of the material is exceeded, the material will "flow". For soft body impact, it will be assumed that the stresses throughout the impact event greatly exceed the material strength, so that the flow will continue indefinitely. After several reflections of the release waves, a condition of steady flow is established. A constant pressure and velocity field is set up in the projectile, and the particles flow along paths which are fixed in space, called streamlines [27].

Using a hydrodynamic impact theory and considering a homogeneous, right-circular cylinder impacting normally on a rigid plate, the flow across a shock can be considered one-dimensional and adiabatic. A short time after the initial shock wave propagates, the equations of conservation of mass (continuity) and momentum for materials behind and after the shock wave can be written as:

$$\rho_1 V_{sh} = \rho_2 (V_{sh} - V_p) \quad (9)$$

$$P_1 + \rho_1 V_{sh}^2 = P_2 + \rho_2 (V_{sh} - V_p)^2 \quad (10)$$

where ρ_1, P_1, ρ_2 and P_2 are the density and pressure of material before and behind the shock wave. V_{sh} is the velocity of the shock propagating into the fluid and V_p is the velocity of the particles behind the shock. For a circular cylinder it can be proved that V_p is equal to the initial velocity of bird V_i. Combining Eqs. (9) and (10) and by defining the Huguenot pressure as $P_H = P_2 - P_1$, the pressure behind the shock is found to be:

$$P_H = \rho_1 V_{sh} V_i \quad (11)$$

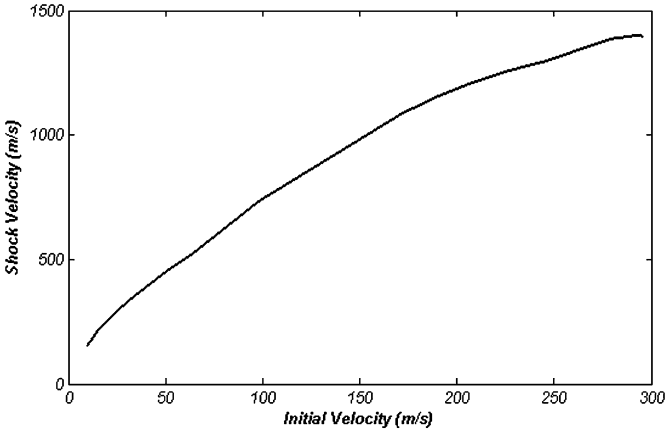

Fig. 3. Variation of shock velocity versus initial velocity for a right-ended cylinder with porosity of 10%.

The proportion of densities before and after impact can be derived from:

$$\frac{\rho_1}{\rho_2} = (1-\alpha)\left(\frac{P_H}{c_1}+1\right)^{-\frac{1}{c_2}} \tag{12}$$

with constants:

$$c_1 = \frac{\rho_1 c_0^2}{4k-1} \tag{13}$$

$$c_2 = 4k-1 \tag{14}$$

where k is an experimental constant, c_0 is the speed of sound in material and α is the porosity of material. Wilbeck found out that a bird can best be described as a low strength material with an average density of 950 $\mathrm{kg\,m^{-3}}$ and 10% porosity, i.e. $\alpha = 0.1$. By solving Eqs. (9) and (12) simultaneously and replacing P_H from (11) into (12), the shock velocity can be obtained by the nonlinear equation:

$$\frac{V_{sh}}{V_{sh}-V_i} = (1-\alpha)\left(\frac{V_{sh}V_i(4k-1)}{c_0^2}\right)^{-\frac{1}{4k-1}} \tag{15}$$

As it can be seen from Eq. (15), the shock velocity is a function of initial velocity. By solving Eq. (15) for V_{sh}, Fig. 3 for shock velocity as a function of initial velocity is obtained.

In the steady-state condition, since the bird materials flow in streamlines, using Bernoulli's equation, the stagnation pressure at the center of impact is found by:

$$P_{stag} = \frac{1}{2}\rho V_i^2 \tag{16}$$

For the test considered, having the initial velocity of $V_i = 116\ \mathrm{m\,s^{-1}}$ and initial density of $\rho_1 = 950\ \mathrm{kg\,m^{-3}}$, using Eqs. (11) and (16), Huguenot pressure and Stagnation pressure are theoretically found to be 88 MPa and 6 MPa, respectively. These values for the experimental test (Fig. 2) are respectively 23 MPa and 5 MPa while it is 37 and 6 MPa for the new FE bird model used (the simulation results are given under Subsection 5.2). The inconsistency in theoretical and experimental values can be attributed to the limitations in the response of pressure gages. In fact, while the Huguenot pressure peak takes place in a very short time, the 100 kHz frequency response of the transducers prevents them from measurement of rise times of less than 5 μs. In FE simulations, 100 kHz frequency has also been chosen for gauges response.

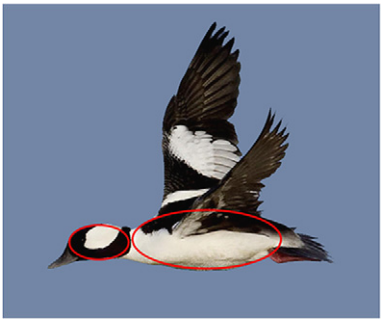

Fig. 4. A typical flying Bufflehead. (For interpretation of the references to color in this figure legend, the reader is referred to the web version of this article.)

Table 1
Bird geometrical specifications.

Bird head-to-tail length	18.7 cm
Bird torso radius	5.4 cm
Head radius	2.7 cm
Wing span	31 cm

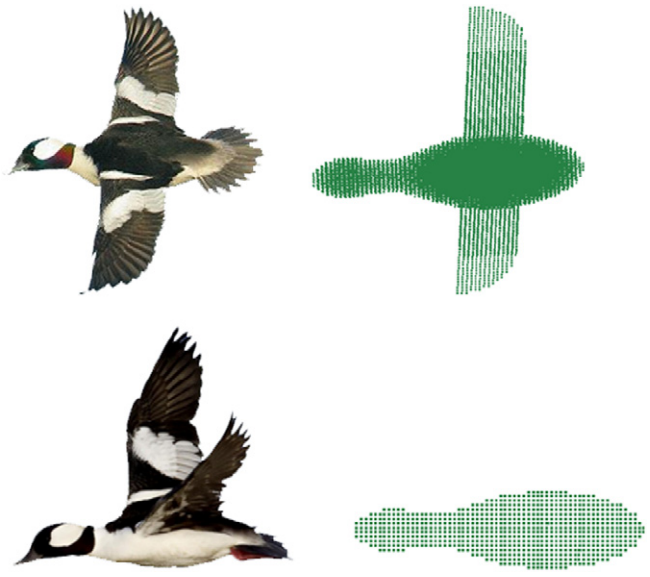

Fig. 5. A real Bufflehead compared to its SPH model.

4. A realistic bird model

4.1. Bird model geometry

In Fig. 4, a typical flying Bufflehead is shown. Two red contours show how the body of a Bufflehead can be simplified. As already mentioned, for the realistic bird model and all other models introduced in this paper, only the SPH method is used.

The model bird is 0.3 kg, and has a length of 0.187 m and a wing span of 0.31 m. The geometrical dimensions considered for the bird model are more specified in Table 1. It is assumed that at the time of impact, the wings are completely spread. In Fig. 5 the real Bufflehead is compared to its SPH model from two views. The SPH bird model consists of 16 284 SPH elements. The distance between two adjacent SPH elements is chosen to be 3 mm.

The bird is hit to the target from 4 different orientations: head, tail, bottom and wing. The position of sensors with respect to the SPH bird model is shown in Fig. 6. For impact from head, tail and bottom side, four sensors were attached on the target. For the wing side, seven sensors were mounted on the target in order to capture the pressure profile in both x and y directions.

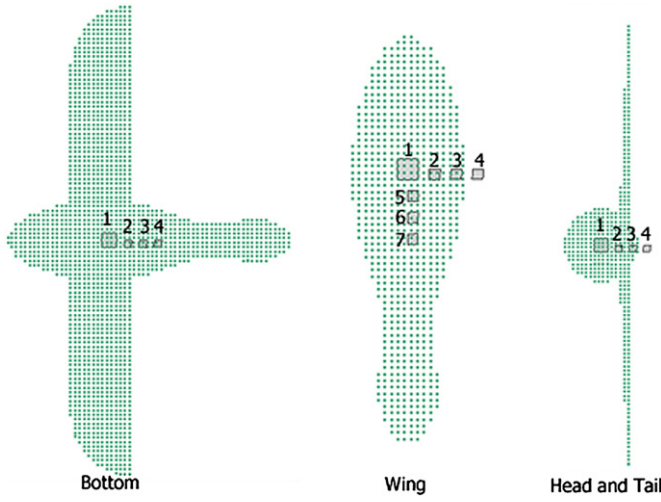

Fig. 6. Position of sensors with respect to the SPH bird model in impacts with different orientations.

4.2. Bird material model

At high impact velocities, in which most fatal bird strikes take place, the bird behaves like a fluid and therefore a hydrodynamic material model can be used for the bird with a reasonable approximation. Thus, a null material model with an Equation of State (EOS) was employed for the SPH bird constitutive modeling. It is noteworthy that the null material model allows only the isotropic components of the stress tensor.

Various equations of states have been proposed for the bird so far: Polynomial, Tabulated and Gruneisen. However, in this study a parametric study was conducted and it was found that a Gruneisen equation of state can best predict the behavior of bird in bird strike impacts. Gruneisen equation (also called $v_s - v_p$ equation of state) describes a linear relationship between the shock and particle velocities. In this study, for the bird a null material model with Gruneisen EOS was used. Gruneisen EOS with cubic shock velocity defines pressure for compressed materials as [14]:

$$P = \frac{\rho_0 C^2 \mu \left[1 + (1 - \frac{\gamma_0}{2})\mu - \frac{a}{2}\mu^2\right]}{\left[1 - (S_1 - 1)\mu - S_2 \frac{\mu^2}{\mu+1} - S_3 \frac{\mu^3}{(\mu+1)^2}\right]^2} + (\gamma_0 + a\mu)E \quad (9)$$

and for expanded material as:

$$P = \rho_0 C^2 \mu + (\gamma_0 + a\mu)E \quad (10)$$

where C is the intercept of the $v_s - v_p$ curve; $S1$, $S2$ and $S3$ are the coefficients of the slope of the $v_s - v_p$ curve; γ_0 is the Gruneisen gamma; and $\mu = \rho/\rho_i - 1$ where ρ is the material density.

For the water Gruneisen equation of state, parameters $C = 1480$ and $S_1 = 1.92$ were used and other parameters were set to zero as defined in [4]. In previous numerical simulations, authors have used densities ranged from 900 $\mathrm{kg\,m^{-3}}$ to 950 $\mathrm{kg\,m^{-3}}$ for bird material. Here, a density of 938 $\mathrm{kg\,m^{-3}}$ is used for the realistic and other substitute bird models as it has been used by most authors previously. In a real bird, the wings structures and materials are different from the rest of the body. However, in this study the wings are modeled as the rest of the body – i.e. as a "water" bullet.

4.3. Target specification

A steel plate, 60 cm in diameter and 6 cm in thickness, is used as target for bird impact simulations. Large thickness of the target plate allows it to be considered appropriately as a rigid plate. The target plate is composed of 14 640 solid elements. In addition to that, one 1 cm × 1 cm shell element at the center of target and three 0.25 cm × 0.25 cm shell elements at upper positions are used in order to capture the pressure profile imposed by the bird model onto the target disc. Both the target solid elements and sensors shell elements were given the linear isotropic material model of steel with density of 7800 $\mathrm{kg\,m^{-3}}$, Young Modulus of 207 GPa and Poisson's ratio of 0.3. The target and the positions of four sensors are shown in Fig. 7.

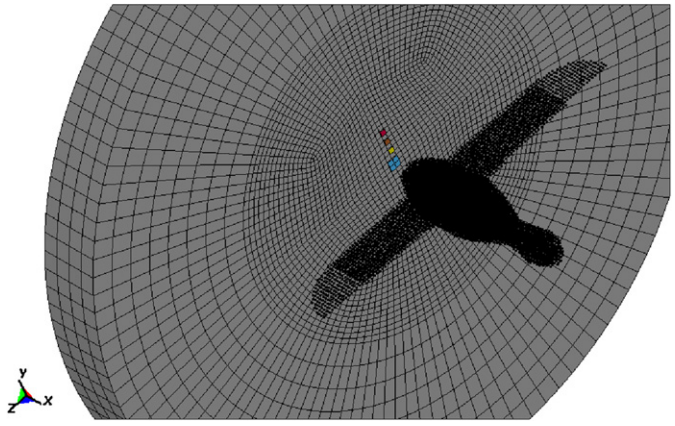

Fig. 7. Setup of bird and target with the positions of four sensors.

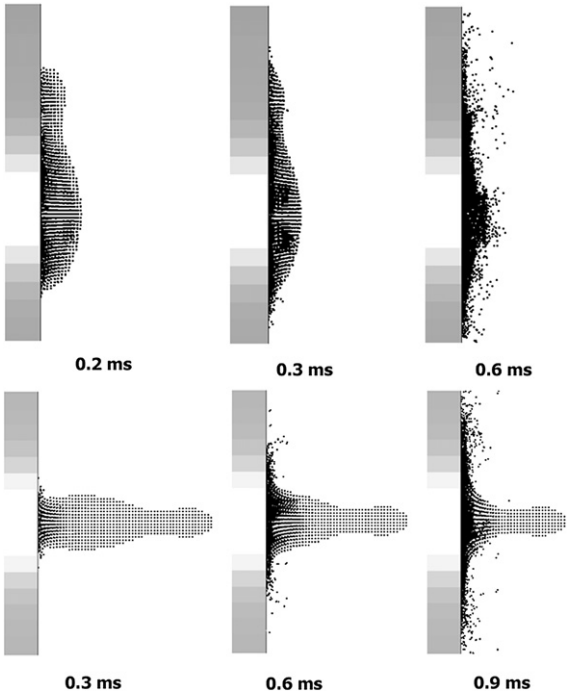

Fig. 8. Deformation of SPH bird model at different times for the birds impacting the target from bottom side (first row) and tail side (second row).

In all calculations, a node to surface contact algorithm was used in order to model the contact between the bird and the rigid target. All the nodes placed on the SPH particles were used as the slave set and all the external segments of target plate elements were used as the master set.

5. Results and discussion

Deformation of SPH bird model at different time instants for the birds impacting the target from tail and bottom sides are shown in Fig. 8.

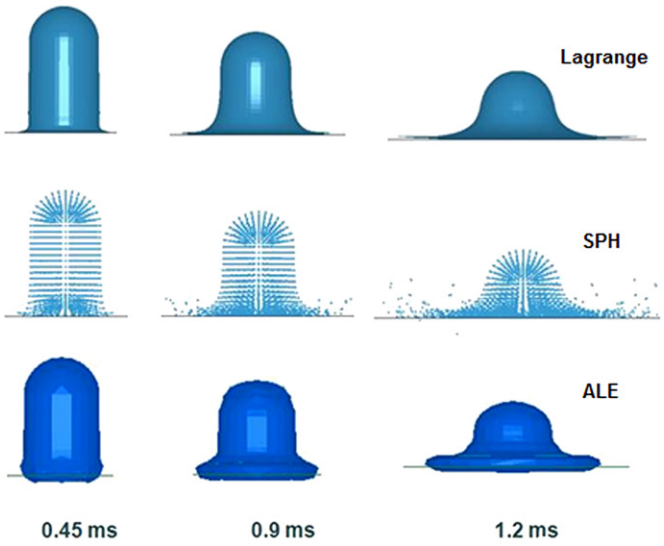

Fig. 9. Deformation of different bird models in the perpendicular impact.

5.1. Comparison between the Lagrangian, ALE and SPH formulations

Before selecting the appropriate formulation for the bird strike simulations, a comprehensive set of simulations were carried out. Three types of bird formulations, i.e. Lagrangian, ALE and SPH were considered. The hemispherical-ended cylinder bird models were created and then impacted to perpendicular rigid target plates. The pressure profiles were compared to Wilbeck experimental test. A steel plate, previously described in Subsection 4.3 is used as the target for all bird impact simulations. Large thickness of the target plate allows it to be considered appropriately as a rigid plate. Since the target is assumed to be rigid and not allowed to have large deformations, dimensions and specifications used for the target are not crucial. In fact, the pressures captured by the sensors are of interest and not the target deformation itself. In this section the bird was modeled as a water projectile with the shape of a hemispherical-ended cylinder with a length to diameter ratio of 2. The impact velocity was set to 116 m/s.

The deformation of the bird model obtained from different formulations with respect to time can be seen in Fig. 9. The pressure profile at the center of the impact for three formulations and for different elements size are depicted in Fig. 10(a)–(c).

As it can be seen from the figures, all the three methods predict relatively close results for fine mesh in comparison to each other as well as to the experimental tests. Anyway for this study the SPH method was selected due to the following reasons: The SPH elements can be defined on the vertexes of same dimensioned adjacent cubes, thus, the mesh is uniform and homogeneous in all directions, i.e. the distance between two neighbor nodes is the same at any position in a simple or complex SPH bird model, while for a complex Lagrangian or ALE bird model the size of elements at various parts is essentially different, especially for a complex geometry. By adopting the SPH bird model, the mesh does not affect the results when the bird impacts the target from its different parts. Therefore, hereafter in this paper, all the simulations were conducted using the SPH method.

5.2. Validation of the realistic bird model

In Wilbeck experimental tests, all birds were launched tail leading and impacted the plate in that orientation for increasing the stability of bird after being shot. In order to validate the new bird model, the results from the realistic bird impacting the target plate from its tail side are compared with the Wilbeck experimental data.

Pressure profile at the center of impact is the most crucial criterion for proving the accuracy of a bird model. The pressure profiles at the center of impact for the impact from tail side and the hemispherical-ended bird model have been compared to the Wilbeck experimental results in Fig. 11. For the sake of brevity, specifications of hemispherical-ended bird model are not presented here, but will be explained in Section 6. As it can be seen, the hemispherical-ended cylinder model, the realistic bird model, and Wilbeck test have the pressure peak of 79, 37 and 23 MPa, respectively. When the bird impacts the target from the tail side, the pressure profile correlates well with Wilbeck test results, while the hemispherical-ended cylinder bird model predicts much higher pressure peak. Therefore, one can conclude that the new bird model can better predict the behavior of bird.

Initial contact area has a significant effect on the Huguenot pressure in each impact scenario. The larger the initial contact area is the higher the Huguenot pressure will be. It is because when the initial contact area is larger, the material at the initial contact area is more limited by the neighbor particles. These neighbor particles prevent the materials at the initial contact area to move outward which then causes the Huguenot pressure increase. As it can be seen from Fig. 6, the initial contact area of the head side impact is larger than that in the tail-side impact. That is why the head-side peak pressure is higher. The new bird model tail side has smaller initial contact area than that of the hemispherical-ended cylinder. That is why the peak pressure of the new bird model is lower than that of the hemispherical-ended cylinder.

The other criterion which is commonly used to validate the numerical bird model is the distribution of stagnation pressure on the target (Fig. 12). The stagnation pressure value at the center of impact for the realistic bird model, Wilbeck experiment and theory (Eq. (8)) are 6 MPa, 5 MPa and 6 MPa, respectively. These values are in a good agreement with each other.

5.3. Effect of bird orientation on pressure distribution

The pressure plots corresponding to four sensors for impacts with different orientations are shown in Fig. 13(a)–(d). For impact from the bottom side, three sensors reach pressures more than 120 MPa while the sensor which is placed far from the center of impact reaches the peak pressure of 42 MPa (see Fig. 13(a)). After 0.7 ms, pressures captured by all sensors diminish. For all sensors after the initial peak pressure, a phase of substantially steady flow is developed. This is because after the initial shock waves developed by the first touch between the bird and target, the shock constantly gets weakened. For a low velocity impact (subsonic), the shock wave will be weakened to the point that it will disappear.

For impact from the head side, the central sensor reaches the peak pressure of 104 MPa when other sensors do not reach pressures more than 25 MPa (Fig. 13(b)). The duration of impact for the impact from the head side is much longer than the impact from the bottom side. This is because the dimension of a bird is much longer from head to tail than from the bottom to the top. The central sensor captures an initial pressure peak and then a phase of steady flow. However, other sensors do not capture an initial pressure peak and in turn, show a steady flow pressure during the impact process.

For the impact from the tail side, the pressure profile is similar to that of the impact from the head side (Fig. 13(c)). One of the differences is that the central sensor captures much lower pressure than that of the head side (38 MPa versus 104 MPa) when other sensors capture higher pressure peaks. It can be concluded that in impact from the tail side, the slope of variation of pressure peak

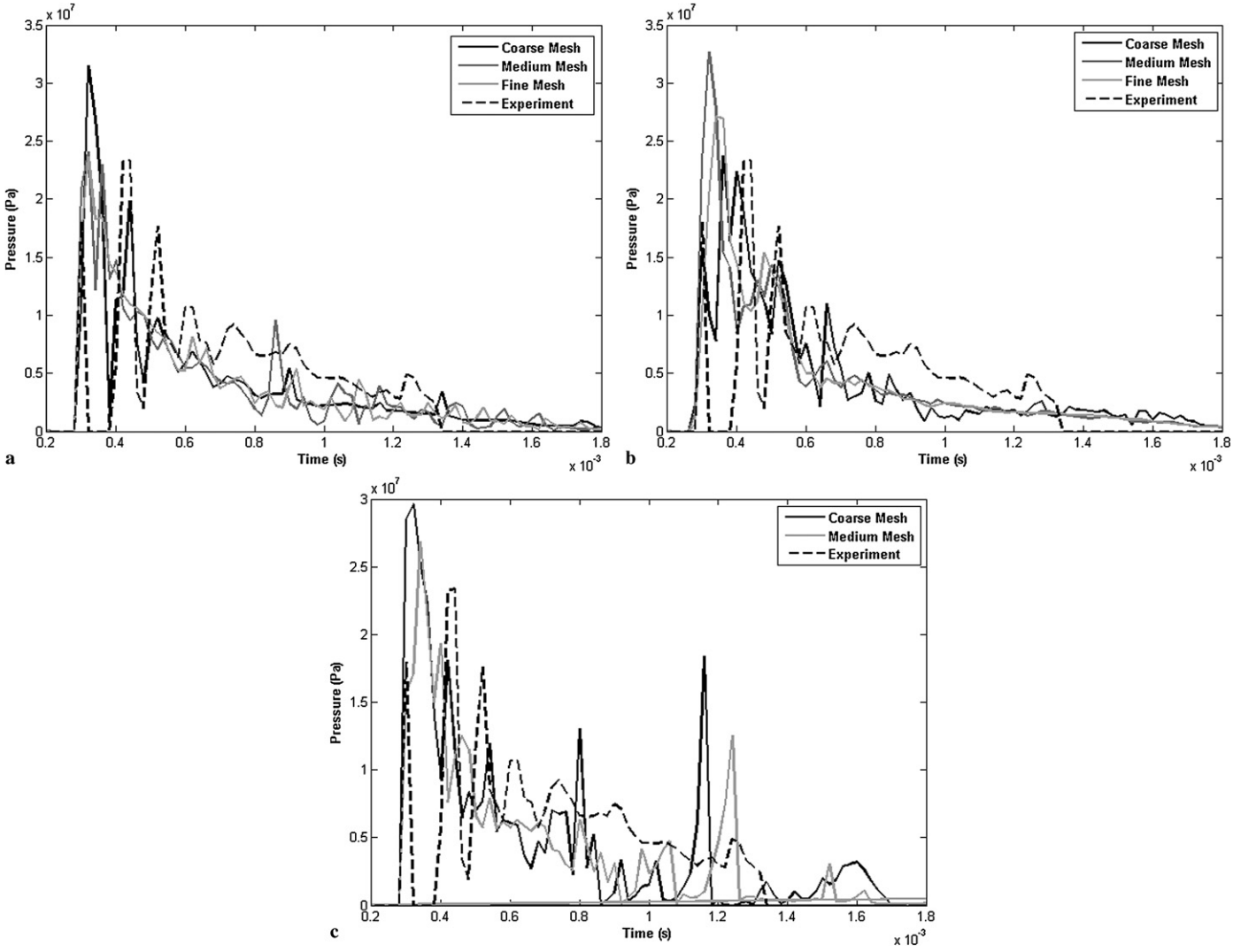

Fig. 10. Pressure profile at the center of impact for (a) Lagrangian formulation, (b) SPH formulation, and (c) ALE formulation.

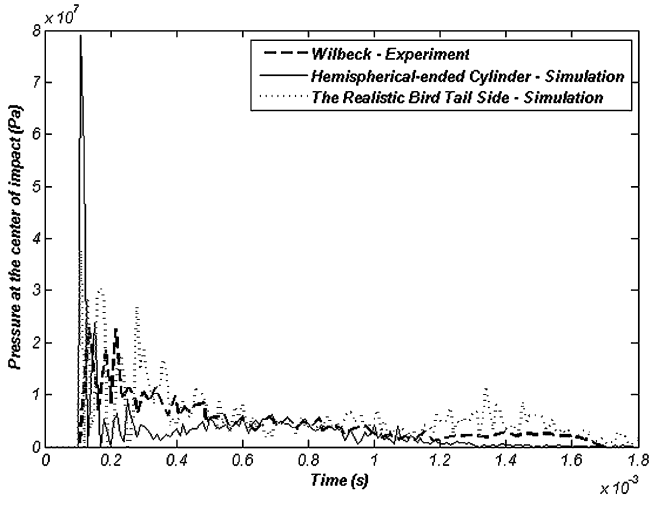

Fig. 11. Pressure profile at the center of impact for old and new bird models compared to experimental result.

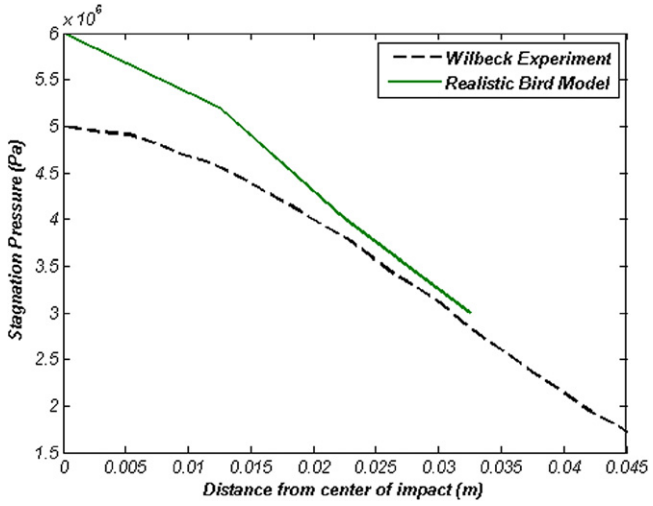

Fig. 12. Distribution of stagnation pressure on the target.

on the plate is much lower than that of the impact from the head side. It can also be seen that in the impact from tail side, all the sensors show a phase of substantially steady flow after an initial peak of pressure.

The pressure profile for the wing side shows that the pressure is higher for the tail-to-head direction as compared with the torso-to-wing direction (Fig. 13(d)). It can also be derived from Fig. 16 that pressure profiles for all the sensors reach their highest point

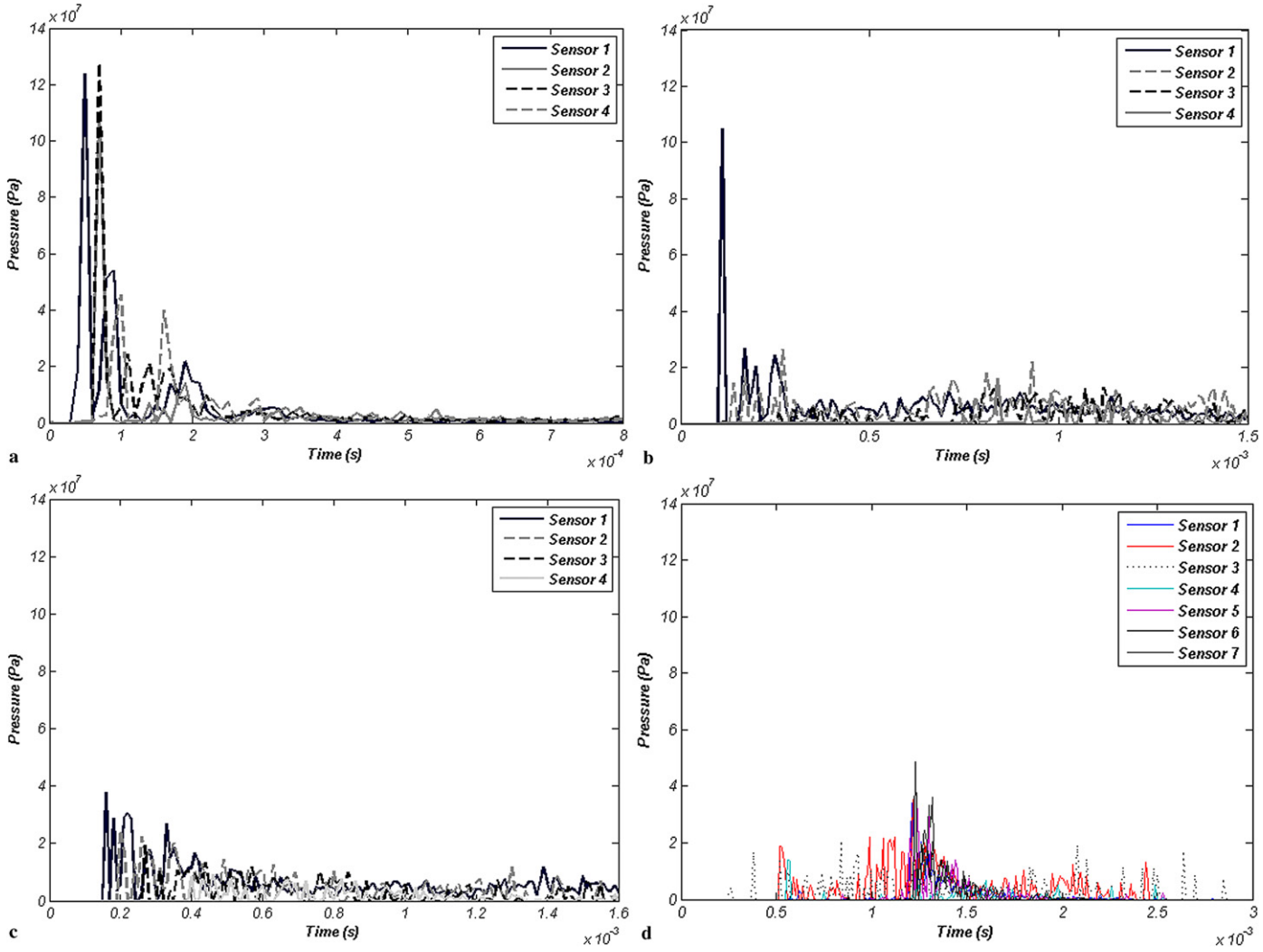

Fig. 13. Pressure profiles captured by sensors 1 to 4 for the impact from (a) bottom side, (b) head side, (c) tail side, and (d) wing side.

when the torso of bird starts to impact the target. Sensors 3, 2 and 4 start propagating earlier and their signals diminish later than other sensors. This is because they are closer to the tip of the tail.

5.4. Pressure peak distribution for impacts with different bird orientations

In Fig. 14, the peak pressure imposed on the target plate is plotted versus distance from the center of the impact. The trend for variations in pressure profile is similar for all the impacts, i.e. for all the impacts, the pressure peak value is maximum at the center of target and decreases when the distance from the center increases. It can also be seen that the peak pressure profile for the bird impacting from the tail correlates relatively well with that of the hemispherical-ended cylinder bird model. It is obvious that during the impact, in which the bird impacts the target from bottom side, three sensors reach peak pressures of 120 MPa. By comparing it with the impacts from other sides, it can be concluded that the highest pressure is formed on the target when the bird impacted it from its bottom side. In other words, for other impact cases, the pressure peak is lower for sensors located far from the center of the target. It is also notable that the bottom side, head side, hemispherical-ended cylinder model, wing side and tail side impose the higher pressure on the target, respectively. This is an important point because it can be concluded that when the bird impacts the target from the tail side, it imposes the lowest pressure peak than in other impact cases. It can, therefore, be careless to consider the experimental/numerical results from the tail side impact as a criterion for designing aircraft components resistant enough against bird strike.

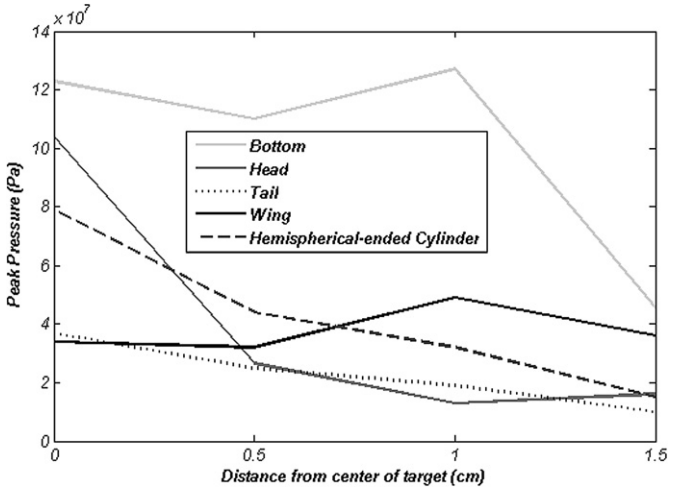

Fig. 14. Peak pressures of sensors in impacts with different orientations and the hemispherical-ended cylinder bird strike modeling.

Based on the FE simulations, it can be concluded that the impact from the bird bottom side is the most damaging scenario, while the tail side impact is the less dangerous one. The peak pressure for the bottom side is 128 MPa while for the tail side it is 38 MPa. For bottom scenario, three sensors reach pressures more than 120 MPa, while for the tail scenario three sensors have the peak pressure of lower than 25 MPa. Therefore, changes in traditional bird models used for the bird strike analysis seem necessary in order to better simulate realistic bird strike events.

Although the peak pressure is much lower in tail-side impact in comparison with the bottom side impact, but the impact duration in tail-side impact is longer which, on the other hand, can increase the damage level as well. The shorter the impact duration is, the more vulnerable the impacted structure is to local penetration. As the impact duration gets longer, the global deformation of the structure becomes more significant. Therefore for the impact of bird to the structure of an aircraft, the simulations or tests must be carried out to find out which parameter (pressure peak or impact duration) has more influence on the integrity of the impacted structure and as a result the worst impact scenario will be found. Since in most bird strike events, the local penetration is the main reason for damage, therefore it can still be concluded that the bottom side impact is the most damaging scenario.

In the next section, four substitute bird models are introduced and their results are studied. The aim is to introduce a proper substitute which is simple, accurate enough and needs less computational efforts in comparison to a realistic bird model.

6. Substitute bird model

From Section 5, it was found that the impact from bird bottom side is the most damaging scenario, while the tail side impact is the less dangerous one. In bird strike simulations in which a bird impacts front facing aircraft components like windshield, wing leading edge and compressor blades, it is time consuming to always model a bird with geometry similar to a real bird which has the organs head, neck and wings. In addition to that, not all birds have the same body shapes or the same dimensions. Therefore, a substitute bird model which can be used as a reference bird model in different situations seems to be necessary. The substitute bird model should be able to predict the pressure distribution on the targets appropriately when impacting from the tail or bottom side. Until now, three bird configurations have been proposed as a substitute for real birds and their results have been compared to Wilbeck's experimental results [27]. The problem is that the three substitute results have been compared to experimental results from the tail side impact. In the current study, four different configurations, namely: sphere, straight-ended cylinder, hemispherical-ended cylinder and ellipsoid were selected and their results are compared to each other and also to Wilbeck experimental results when impacting from the tail side. The four configuration results are also compared to the more realistic bird model introduced in Section 5 when impacting from the bottom side and tail side.

6.1. Bird and target discretization

For all the configurations except for the sphere, a length-to-diameter ratio of two was selected, as suggested by previous works [13]. For the considered mass of 0.3 kg, the diameters 0.0647, 0.0626, 0.0588 and 0.0848 m are obtained for ellipsoid, hemispherical-ended cylinder, straight-ended cylinder, and sphere, respectively. Various SPH bird model are shown in Fig. 15. The number next to each bird model shows the number of its SPH elements. Similar to previous simulations, the null material model with Gruneisen equation of state is employed for all models. Moreover, the target and sensor elements have the same dimensions and the material parameters are the same as the previous simulations.

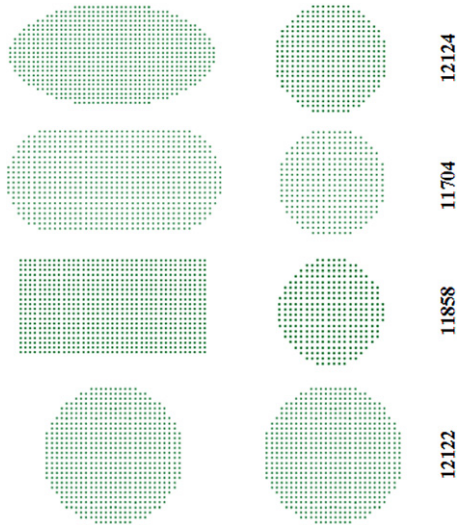

Fig. 15. Various SPH bird models – number of SPH elements.

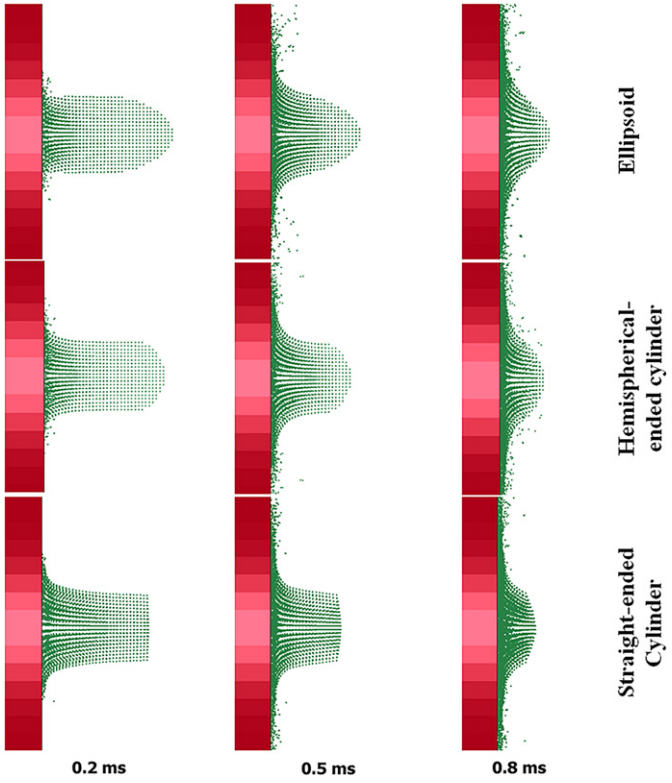

Fig. 16. Deformation of different bird configurations at different time intervals for the impact from tail side.

6.2. Tail side impact results

Since the tail side impact for different bird models has been previously discussed by other authors [18,13], the results of tail side impact for various substitute bird models will be presented briefly. Deformation of different bird configurations at different time intervals is shown in Fig. 16. The deformation of different

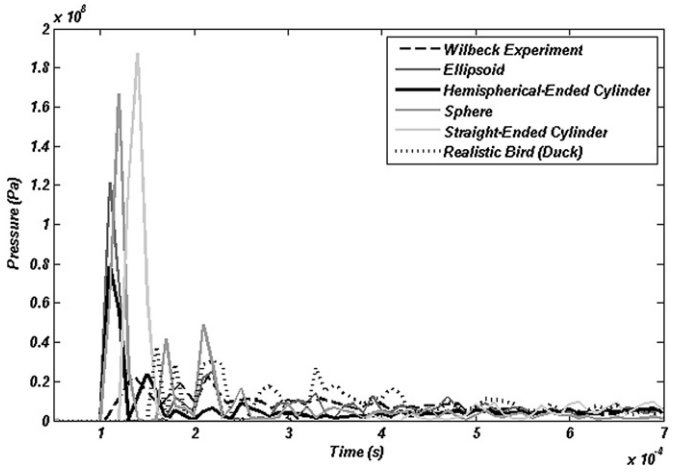

Fig. 17. Pressure at the center of impact for Wilbeck experimental result, the realistic bird model and substitute bird configurations.

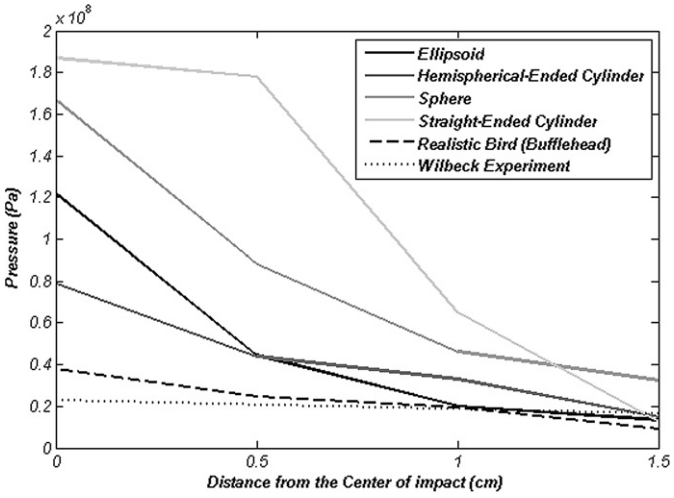

Fig. 18. The peak of pressure imposed on the target plate versus distance from the center of impact for the tail side impact.

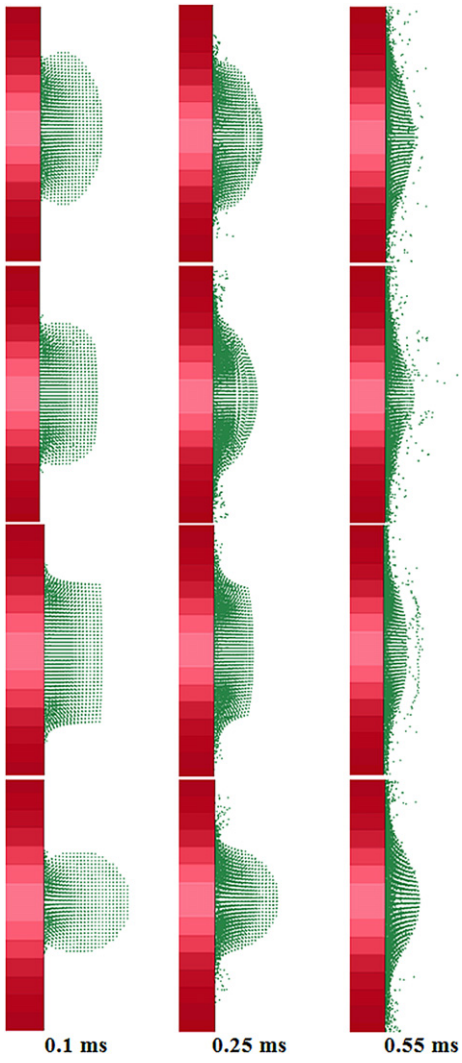

Fig. 19. Deformation of different bird configurations at different time intervals for the impact from bottom side.

bird configurations is different at the initial moments of impact, but then after the middle of impact, they deform in a similar way.

In Fig. 17, pressure at the center of impact is compared for the Wilbeck experimental result, the realistic bird model and four substitute bird configurations. As it can be seen, straight-ended cylinder and sphere predict pressure profiles much higher than Wilbeck experimental result. Ellipsoid, also, predicts a high pressure peak, although its peak pressure is more accurate than that of sphere and straight-ended cylinder. Among the four bird configurations, the hemispherical-ended cylinder predicts a pressure peak closer to the experimental result. It is notable that the realistic bird model, predicts the best pressure peak in comparison with other numerical models. It is because its initial contact area is more similar to a real bird than that of other geometries.

In Fig. 18, the peak of pressure imposed on the target plate is plotted versus distance from the center of impact. The trend for variations in pressure peak is similar for all the impacts, i.e. for all the impacts, the pressure peak is maximum at the center of target and it decreases when the distance from the center increases. Again, the straight-ended cylinder and the sphere predict pressure distribution much higher than the realistic bird model. Ellipsoid and hemispherical-ended cylinder correlate better with Wilbeck experiment, while the hemispherical-ended cylinder seems to be the most accurate model among presented substitute bird models. The peak pressure at the center of impact for the hemispherical-ended cylinder is 80 MPa, while for the realistic bird model and Wilbeck experiment it is 38 MPa and 24 MPa, respectively.

6.3. Bottom side impact results

As concluded earlier in the paper, the bottom side impact is the most damaging scenario in a bird strike event. Deformation of different bird configurations at different time intervals is shown in Fig. 19.

Pressure–time curves captured by four sensors for different substitute bird configurations are plotted in Figs. 20(a)–(c). Pressure profile distribution for the ellipsoid is shown in Fig. 20(a). In the impact of ellipsoid bird model to the rigid target, the three central sensors reach their higher peaks at the same time while the fourth sensor reaches its highest value after a short delay. It is also notable that the central sensor has the pressure peak of 155 MPa while the three other sensors show a maximum pressure of approximately 120 MPa. All the sensors show a phase of steady state show after the initial shock phase.

In Fig. 20(b), pressure profiles recorded by sensors 1 to 4 are shown for hemispherical-ended cylinder. As it can be seen, all sensors reach their highest values at the same time. This can be attributed to the shape of hemispherical-ended cylinder which is flat at sides and as a result starts to touch all the sensors at the same time. Sensors 1 to 3 have the maximum pressures of more than

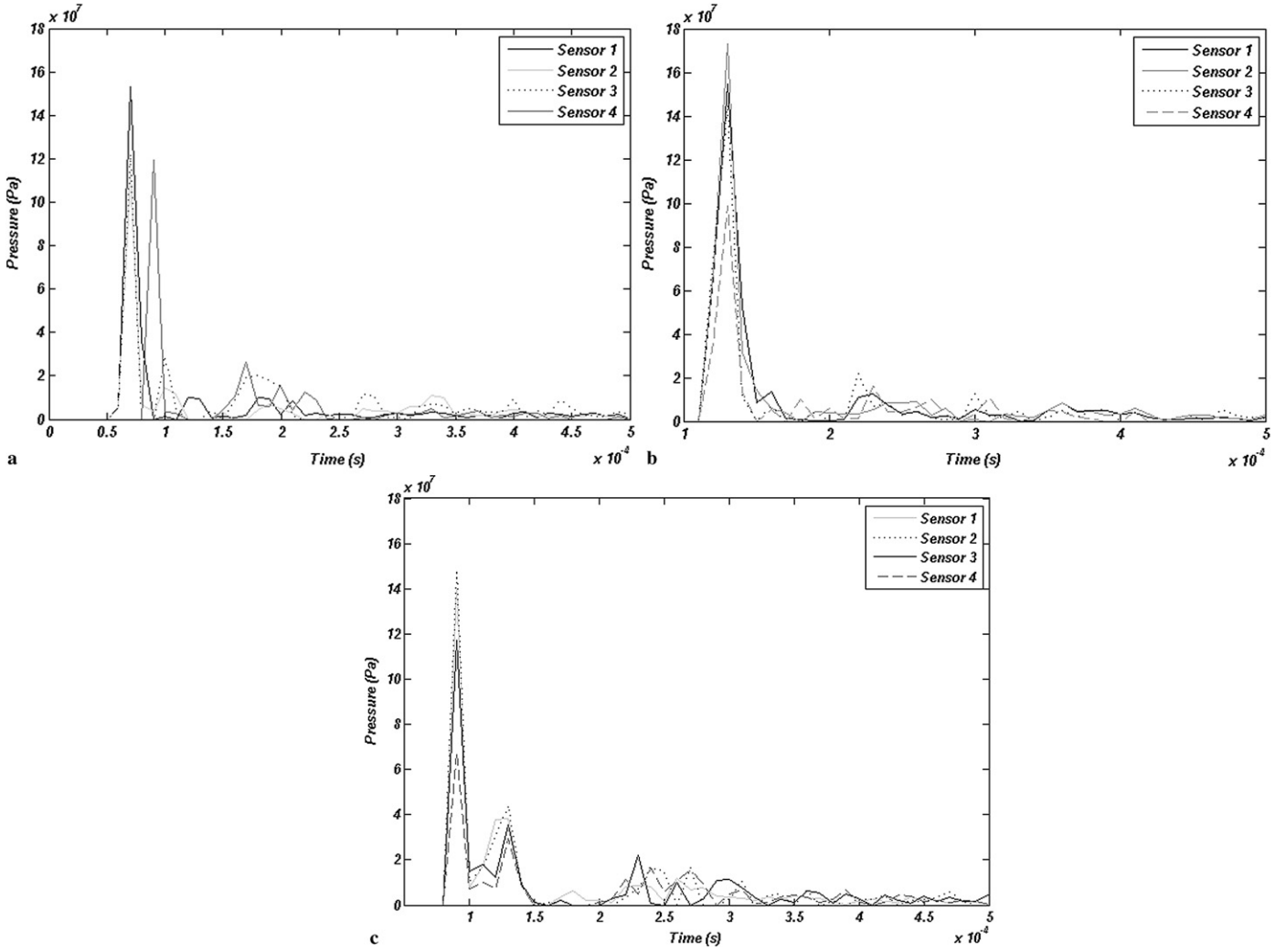

Fig. 20. Pressure profiles captured by sensors 1 to 4 for the impact of (a) ellipsoid, (b) hemispherical-ended, (c) straight-ended bird model.

140 MPa, while the 4th sensor has the peak pressure of 95 MPa only.

In Fig. 20(c), pressure profiles recorded by sensors 1 to 4 are shown for the case of straight-ended cylinder. In this impact, like the hemispherical-ended cylinder, all the sensors reach their highest values at the same time. This is because straight-ended cylinder, like the hemispherical-ended cylinder, has a flat surface in the longitudinal side. Again, sensors 1 to 3 have the maximum pressures of more than 120 MPa, while the 4th sensor has a pressure peak of 70 MPa.

In Fig. 21, distribution of maximum pressures for different bird substitutes are shown and compared to each other, as well as to that of the realistic bird impacting from its bottom side. The sphere configuration pressure distribution is different from other configurations. It also shows a significant deviation from the realistic bird model. Therefore, it can be concluded that it is an unsuitable substitute for real birds. Hemispherical-ended cylinder and straight-ended cylinder both predict peak pressures higher than the realistic bird model. On the other hand, the ellipsoid bird model maximum pressure distribution shows a good correlation with that of the realistic bird model. One may conclude that the ellipsoid bird model can more precisely model the pressure distribution imposed on the target.

According to the results from impacts from tail and bottom side by different bird configurations, it can be concluded that the sphere and straight-ended cylinder have imprecise results in impacts from both the tail and bottom side. Comparing the two remaining configurations, the hemispherical-ended cylinder creates more accurate result when impacting from the tail side, while it shows inferior results in the impact from the bottom side. On the other hand, the ellipsoid correlates well with the experimental result, when impacting from the bottom side, but does not

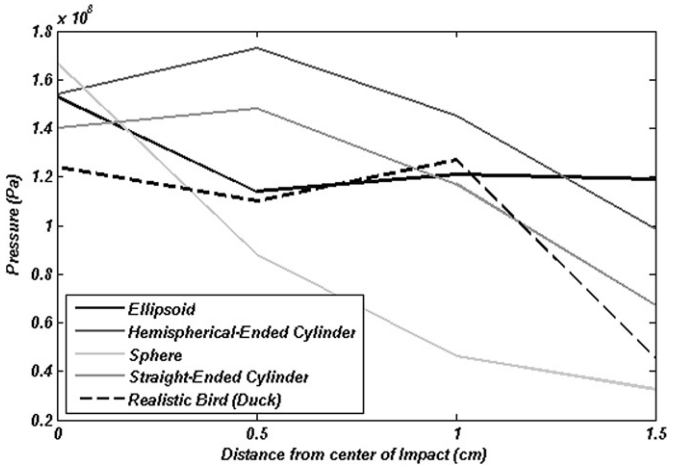

Fig. 21. Distribution of maximum pressures for different bird substitutes and the realistic bird impacting from bottom side.

indicate a comparatively accurate result when impacting from the tail side.

7. Conclusions

In experimental tests of bird impact, birds are usually launched tail leading and are impacted to the target in that orientation for increasing the stability of shooting. On the other hand, in the real bird strike events the birds do not always impact a surface from the tail side orientation. In this study, using a SPH realistic bird model, the effect of orientation in bird strike events is investigated. Based on the FE simulation, it can be concluded that the impact from bird bottom side is the most damaging scenario while the tail side impact is a less dangerous one. The pressure peak for the bottom side impact is about three times of that in the impact from tail side. Generally it was found that the bottom side, head side, hemispherical-ended cylinder model, wing side and tail side impose the higher pressure on the target, respectively. This is an important point because it can be concluded that when the bird impacts the target from the tail side, it imposes the lowest pressure peak than in other impact cases. It can, therefore, be careless to consider the experimental/numerical results from the tail side impact as a criterion for designing aircraft components resistant enough against bird strike. Therefore, changes in traditional bird models used for bird strike analysis are necessary in order to better simulate real bird strike events.

In bird strike simulations in which a bird impacts aircraft components such as windshield, wing leading edge or compressor blades, it is time consuming to always model a bird with geometry similar to a real bird which has the organs head, neck and wings. In addition to that, not all the birds have the same body shapes nor the same dimensions. Therefore, a substitute bird model which can be used as a reference bird model for different problems is necessary. Four substitute bird models, namely, sphere, straight-ended cylinder, hemispherical-ended cylinder and ellipsoid were presented and their results were analyzed. It was found that for the tail side impact scenario, the hemispherical-ended cylinder shows the best results, while for the bottom side impact scenario, the ellipsoid can be the best candidate for the bird substitute model. If it is necessary to choose only one of the configurations to model impacts from different orientations, it is suggested to select the ellipsoid. It is because of two reasons: first, in the tail side impact of ellipsoid, the pressure peak is inaccurate only for the central sensor, while other sensors show good correlation with experimental data. Second, most birds have an ellipsoid shaped body rather than hemispherical-ended cylinder.

References

[1] A. Airoldi, B. Cacchione, Modelling of impact forces and pressures in Lagrangian bird strike analyses, Int. J. Impact Eng. 32 (2006) 1651–1677.
[2] J.P. Barber, H.R. Taylor, J.S. Wilbeck, Characterization of bird impacts on a rigid plate: Part I, University of Dayton Research Institute, Technical Report AFFDL-TR-75-5, 1975.
[3] R.A. Brockman, T.W. Held, Explicit finite element method for transparency impact analysis, University of Dayton Research Institute Report WL-TR-91-3006, 1991.
[4] M. Chizari, L.M. Barrett, S.T.S. Al-Hassani, An explicit numerical modeling of the water jet tube forming, Comput. Mater. Sci. 45 (2009) 378–384.
[5] E. Cleary, Wildlife strikes to civil aircraft in the United States 1990–2004, Federal Aviation Administration National Wildlife Strike Database, No. 11, 2005.
[6] J. Frischbier, Bird strike capability of a transonic fan blisk, in: Proceedings of the ASME Turboexpo, Orlando, FL, June 1997, pp. 2–5.
[7] Y.P. Guan, W. Chen, Z.Y. Huang, Sliced model for bird impacting blades, J. Nanjing Univ. Aeronaut. Astronaut. 36 (6) (2004) 784–786.
[8] A.G. Hanssen, Y. Girard, L. Olovsson, T. Berstad, M. Langseth, A numerical model for bird strike of aluminium foam-based sandwich panels, Int. J. Impact Eng. 32 (2006) 1127–1144.
[9] P. Hut, L. Hernquist, G. Lake, J. Makino, S. McMillan, T. Sterling, Smooth particle hydrodynamics: Models, applications, and enabling technologies, in: Proceedings form the Workshop Presented by the Institute for Advance Study at Princeton, 1997.
[10] J. Lacome, Smooth Particle Hydrodynamics (SPH): A new feature in LSDYNA, in: Proceedings of the 6th International LS-DYNA Users Conference, Session 7-3, 2000.
[11] J.L. Lacome, Smoothed particle hydrodynamics – Part II, in: FEA Information International News for the World-Wide Engineering Community, 2001, November 27, pp. 6–11.
[12] B. Langrand, A.S. Bayart, Y. Chauveau, E. Deletombe, Assessment of multi-physics FE methods for bird strike modelling—Application to a metallic riveted airframe, Int. J. Crashworth. 7 (4) (2002) 415–428.
[13] M.A. Lavoie, A. Gakwaya, M. NejadEnsan, D.G. Zimcik, Validation of available approaches for numerical bird strike modeling tools, Int. Rev. Mec. Eng. 1 (2007) 380–389.
[14] Livermore software Inc., LS-DYNA Keyword User's Manual, ver. 9.71, Livermore, CA, 2006.
[15] L.B. Lucy, A numerical approach to the testing of the fission hypothesis, Astron. J. 82 (1977) 1013–1020.
[16] N.F. Martin, Nonlinear Finite Element Analysis to Predict Fan Blade Impact Damage, Pratt & Whitney, 2004.
[17] M.A. McCarthy, J.R. Xiao, C.T. McCarthy, A. Kamoulakos, J. Ramos, J.P. Gallard, Modelling of bird strike on an aircraft wing leading edge made from fiber metal laminates—Part 2: Modeling of impact with SPH bird model, Appl. Compos. Mater. 11 (5) (2004) 317–340.
[18] S.A. Meguid, R.H. Mao, T.Y. Ng, FE analysis of geometry effects of an artificial bird striking an aero engine fan blade, Int. J. Impact Eng. 35 (2007) 487–498.
[19] T.J. Moffat, W.L. Cleghorn, Prediction of bird impact pressures and damage using MSC/DYTRAN, in: Proceedings of ASME TURBOEXPO 2001, Louisiana.
[20] J. Monaghan, On the problem of penetration in particle methods, J. Comput. Phys. 82 (1) (May 1989) 1–15.
[21] E. Niering, Simulation of Bird Strikes on Turbine Engines, Turbinen-Union Munich, Germany, 1988.
[22] B. Richard, The development of a substitute artificial bird by the International Bird strike Research Group for use in aircraft component testing, International Bird Strike Committee ISBC25/ WP-IE3 (2000), Amsterdam.
[23] C. Stoker, Developments of the arbitrary Lagrangian–Eulerian method in non-linear solid mechanics, Enschede, The Netherlands, 1999.
[24] F. Stoll, R.A. Brockman, Finite element simulation of high speed soft-body impacts, in: Proceedings of the 1997 38th AIAA/ASME/ASCE/AHS/ASC Structure, Structural Dynamics, and Materials Conference, Part 1 (of 4), Kissimmee, FL, USA, 1997, pp. 334–344.
[25] J. Thorpe, Fatalities and destroyed civil aircraft due to bird strikes, 2002 to 2004, International Bird Strike Committee, Athens, May 2005, pp. 23–27.
[26] L.C. Ubels, A.F. Johnson, J.P. Gallard, M. Sunaric, Design and testing of a composite bird strike resistant leading edge, in: SAMPE Europe Conference Exhibition, National Aerospace Laboratory, 2003.
[27] J. Wilbeck, Impact behavior of low strength projectiles, Report No. AFML-TR-77–134, Air Force Materials Lab., Air Force Wright Aeronautical Lab's, Wright-Patterson Air Force base, OH, 1977.